

Blood Clearance, Distribution, Transformation, Excretion, and Toxicity of Near-Infrared Quantum Dots Ag_2Se in Mice

Huan Tang,[†] Sheng-Tao Yang,[‡] Yi-Fan Yang,[§] Da-Ming Ke,[§] Jia-Hui Liu,[†] Xing Chen,[†] Haifang Wang,^{*,§} and Yuanfang Liu^{*,†,§}

[†] Beijing National Laboratory for Molecular Sciences, Department of Chemical Biology, College of Chemistry and Molecular Engineering, Peking University, Beijing 100871, China

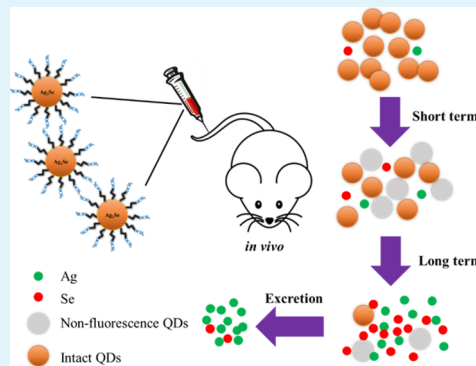
[‡] College of Chemistry and Environment Protection Engineering, Southwest University for Nationalities, Chengdu 610041, China

[§] Institute of Nanochemistry and Nanobiology, Shanghai University, Shanghai 200444, China

Supporting Information

ABSTRACT: As a novel fluorescent probe in the second near-infrared window, Ag_2Se quantum dots (QDs) exhibit great prospect in *in vivo* imaging due to their maximal penetration depth and negligible background. However, the *in vivo* behavior and toxicity of Ag_2Se QDs still largely remain unknown, which severely hinders their wide-ranging biomedical applications. Herein, we systematically studied the blood clearance, distribution, transformation, excretion, and toxicity of polyethylene glycol (PEG) coated Ag_2Se QDs in mice after intravenous administration with a high dose of $8 \mu\text{mol}/\text{kg}$ body weight. QDs are quickly cleared from the blood with a circulation half-life of 0.4 h. QDs mainly accumulate in liver and spleen and are remarkably transformed into Ag and Se within 1 week. Ag is excreted from the body readily through both feces and urine, whereas Se is excreted hardly. The toxicological evaluations demonstrate that there is no overt acute toxicity of Ag_2Se QDs to mice. Moreover, in regard to the *in vivo* stability problem of Ag_2Se QDs, the biotransformation and its related metabolism are intensively discussed, and some promising coating means for Ag_2Se QDs to avert transformation are proposed as well. Our work lays a solid foundation for safe applications of Ag_2Se QDs in bioimaging in the future.

KEYWORDS: Ag_2Se , quantum dots, blood clearance, biodistribution, biotransformation, toxicity



1. INTRODUCTION

Over the past decade, various quantum dots (QDs), typically CdSe QDs and their analogues, have been developed as the fluorescent probes for bioimaging due to their unique optical properties.^{1,2} Compared with conventional organic fluorescent dyes, QDs possess advantages of high quantum yield, good resistance to photobleaching, narrow emission peak, and tunable emission wavelength. Successful demonstrations of bioimaging with QDs have been achieved both *in vitro* and *in vivo*, such as sentinel lymph node mapping, tumor angiogenesis imaging, and neurocyte and virus infection tracking.^{3,4} However, the toxic constituent of traditional QDs is unacceptable for clinical applications, even if these QDs are encapsulated by other substances to block the toxic metal ion release.^{5,6} Moreover, the emission peaks of CdSe QDs and their analogues are usually in the visible range,⁷ which is not optimal for the *in vivo* imaging. Xu et al., therefore, claimed that developing safe and high-performance Cd-free QDs was highly demanded.⁸

Among these newly developed QDs, Ag_2Se QDs are ideal for the *in vivo* imaging, because of the near-infrared (NIR) emission and the Cd-free composition.^{9–11} The emission peak

of Ag_2Se QDs ($\sim 1300 \text{ nm}$) is within the region of the second NIR window (NIR II, 1000–1400 nm), which enables deeper tissue penetration and a higher signal/noise ratio due to the lower photoabsorption and tissue scattering.¹² Several *in vivo* imaging cases of Ag_2Se QDs have been reported. For example, Dong et al. achieved the imaging of liver, spleen, and high-ordered branches of blood vessels with high spatial resolution in mice after intravenous injection of Ag_2Se QDs.¹¹ The NIR-II photoluminescence signals derived from the multidentate-polymer-capping Ag_2Se QDs were also visualized in several regions of the mouse body after they were injected into blood.¹³ In contrast to the good imaging performance, the biocompatibility and safety of Ag_2Se QDs over traditional CdSe QDs have not been validated yet.

Biodistribution and toxicity of Ag_2Se QDs should be carefully studied to guarantee the safe applications *in vivo*, considering the reported discrepancy among studies of QDs at both cell and animal tiers.¹⁴ Previous studies illustrated that Ag_2Se QDs

Received: April 28, 2016

Accepted: June 28, 2016

Published: June 28, 2016

showed negligible side effects at the cellular level,^{10,11} and no apparently abnormal behavior was observed during the *in vivo* imaging.¹³ However, a systematic evaluation of absorption, distribution, metabolism, excretion, and toxicity (ADME/T) of Ag₂Se QDs is scarce to date.

Herein, we systematically investigated the blood clearance, distribution, transformation, excretion, and toxicity of polyethylene glycol (PEG) coated Ag₂Se QDs (denoted as Ag₂Se QDs-PEG) in mice. The Ag and Se contents in blood and other organs were quantified by inductively coupled plasma-mass spectrometry (ICP-MS), and hence, the information on blood clearance, distribution, biotransformation, and excretion was obtained. As supplementary approaches, Ag₂Se QDs-PEG was quantified based on the fluorescence intensity both *in vivo* and *ex vivo*. The organ index, serum biochemistry, and histopathology were monitored to reveal the potential toxicity that will ensure safe applications of Ag₂Se QDs in the future.

2. MATERIALS AND METHODS

2.1. Materials. 1-Dodecanethiol (DT, 98%) and oleylamine (OAM, 80–90%) were purchased from Aladdin Co. (Shanghai, China). Poly(maleicanhydride-*alt*-1-octadecene) (C18-PMH) was obtained from Sigma-Aldrich Co. (USA). Methoxypolyethylene glycol amine (5000 MW) was purchased from Beijing KaiZheng Biotechnology Inc. (China). Selenium powder (99.95%), NaBH₄ (>96%), HNO₃ (MOS grade), H₂O₂ (MOS grade), and AgNO₃ were bought from Sinopharm Chemical Reagent Co., Ltd. (China). All other reagents were of analytical grade and used without further purification.

2.2. Synthesis of Ag₂Se QDs-PEG. Ag₂Se QDs-PEG was synthesized based on oil-soluble DT-coated Ag₂Se QDs (denoted as Ag₂Se QDs-DT) according to the previous report.¹¹ Briefly, NaHSe solution and C18-PMH-PEG were prepared following the protocols as described in the Supporting Information (SI). AgNO₃ (101.92 mg, 0.6 mmol) was dissolved in a mixture of 45 mL of OAM and 105 mL of toluene. Then 45 mL of DT and 105 mL of NaHSe solution (0.15 mmol) were added in order. The obtained mixture was stirred for 5 min and transferred to an autoclave. The solvothermal reaction was performed at 180 °C for 1 h. Upon cooling to room temperature, the product was washed with ethanol three times by centrifugation (12 000 rpm, 5 min). Ag₂Se QDs-DT was redispersed and stored in cyclohexane. Then 150 mg of solid Ag₂Se QDs-DT was dispersed into 30 mL of chloroform with the help of sonication. Finally, 100 mg of C18-PMH-PEG was added and stirred for 12 h at room temperature to produce Ag₂Se QDs-PEG. The solvent was removed by distillation, and Ag₂Se QDs-PEG was transferred into water.

The Ag₂Se QDs-PEG sample was systematically characterized by high-resolution transmission electron microscope (HR-TEM, JEM-2010, JEOL, Japan), X-ray photoelectron spectroscopy spectra (XPS, Axis Ultra, Japan), powder X-ray diffraction (XRD, DMAX-2200, Rigaku, Japan), energy-dispersive X-ray (EDX, JEM-2010, JEOL, Japan) with Genesis software, Fourier transform infrared spectroscopy (FTIR, Nicolet Magna IR 750, Thermal, USA), NIR fluorescence spectroscopy (Nanolog FL3-2iHR, HORIBA, France), dynamic light scattering (DLS, Nano ZS90, Malvern, USA), and inductively coupled plasma-atomic emission spectrometry (ICP-AES, Prodigy, Leeman Laboratories, USA). Considering the relative high concentration of Ag₂Se QDs stock solution (>1 μmol/mL), ICP-AES analysis was used to determine the concentration of Ag₂Se QDs-PEG stock solution, which was digested with HNO₃ and H₂O₂.

2.3. Stability of Ag₂Se QDs-PEG in Simulated Body Fluid (SBF) and Fetal Bovine Serum (FBS). SBF was prepared following the recipe in Table S1.¹⁵ Ag₂Se QDs-PEG (1 μmol/mL) in 1 mL of SBF was transferred into dialysis bags (MWCO 1000 Da) and placed in polypropylene beakers containing 50 mL of SBF. After mild stirring for 2 min, 5 min, 15 min, 30 min, 1 h, 3 h, 6 h, 1 d, 2 d, and 3 d, 1 mL of dialysate was taken out and diluted with 4 mL of 2% HNO₃ for the determination of Ag and Se by ICP-MS (Elan DRC-e, PerkinElmer, USA). After dialysis for 3 d, Ag₂Se QDs-PEG remaining in the dialysis

bag was characterized by TEM and NIR fluorescence spectroscopy. The atomic ratio of Ag₂Se QDs-PEG remaining in the dialysis bag was also determined by ICP-AES. The stability of Ag₂Se QDs-PEG in FBS (Gibco, NY, USA) was investigated in the same way.

2.4. Animal Experiments. All animal experiments were performed in compliance with the institutional ethics committee regulations and guidelines on animal welfare (Animal Care and Use Program Guidelines of Peking University) with the approval by Peking University.

Male CD-1 (ICR) mice (20–25 g) were provided by the Vitalriver Experimental Animal Co. (Beijing, China). The mice were housed under normal laboratory conditions with free access to standard rodent food and water. They were kept on a 12 h light/dark cycle. After acclimation, mice were randomized into groups (5 mice per group). The mice were intravenously injected with Ag₂Se QDs-PEG (1 μmol/mL) in saline at a high dose of 8 μmol/kg body weight (b.w.) (refers to the concentration of Ag element). The dose was set as 8 μmol/kg b.w. for three reasons. First, the imaging doses for Ag₂Se QDs and other QDs usually range from several pmol/kg b.w. to several μmol/kg b.w. Second, the biosafety studies of QDs are conducted at the doses from several pmol/kg b.w. to several μmol/kg b.w. Third, the dose of 8 μmol/kg b.w. is also a necessary concentration to study the fate of Se from Ag₂Se QDs, because only the high dose may overwhelm the high Se background of the originally existed essential element Se in vivo. Mice injected with saline were taken as the control. The body weights were recorded daily for 28 d, and the urine/feces were collected daily, too. Mice were killed and dissected to collect blood and other organs at designed time points (2 min to 28 d). The organ index is the ratio of the weight of the organ to the body weight.

2.5. Blood Clearance and Biodistribution. Biological samples, including blood, heart, liver, spleen, lungs, kidneys and brain, were weighed and transferred into tetrafluoroethylene digestion tubes. Then, 4 mL of HNO₃ and 1 mL of H₂O₂ were added into each tube, and the tubes were kept at 180 °C for 25 min with a microwave digestion system (MARS, CEM Corp., USA). Upon cooling, the solution was diluted by ultrapure water to proper concentrations for Ag and Se analyses by ICP-MS, because of the low accumulation levels of Ag₂Se QDs. To obtain the lower detection threshold of Se contents, Se was measured with a dynamic reaction cell (DRC) using high-purity CH₄ as the carrier gas. For each liver sample it was cut in half and separately digested. Then the two digestion solution samples were merged and diluted by ultrapure water before the ICP-MS measurement.

The efficiency of digestion procedures was tested using the certified reference material, Dogfish Liver, provided by the National Research Council Canada. The obtained recovery rates were 101.7 ± 6.1% for ¹⁰⁹Ag (*n* = 4) and 98.3 ± 3.5% for ⁸⁰Se (*n* = 4). The calibration plot for Ag and Se was prepared with concentrations of 1, 5, 20, and 100 ng/mL, and the correlation coefficients were all above 99.99%. The mean value of the tested elements in the control samples was subtracted as the background for each tested sample.

The kinetic parameters of Ag₂Se QDs-PEG in the blood were calculated using 3P87 software.¹⁶ The accumulation levels in organs were expressed as percentage of the injected dose (% ID) and ng/g wet tissue.

2.6. Ex Vivo and in Vivo Imaging. Ag₂Se QDs-PEG was intravenously administered to male CD-1 mice (20–25 g) at a dose of 8 μmol/kg b.w. At 1 h, 6 h, 24 h, and 48 h postinjection, mice were killed and tissue samples were collected for the *ex vivo* imaging. The imaging parameters were the same as those of the *in vivo* imaging and are described as below.

The male nude mice (CD-1/NU, 20–25 g) were selected for the *in vivo* imaging. During the period of injection and imaging, the mice were anesthetized using 200 μL of 10% chloral hydrate for each. NIR II fluorescence images were collected using a two-dimensional InGaAs array. The excitation light was provided by an 808 nm diode laser and filtered by two short-pass filters (850 and 1000 nm, Thorlabs). The excitation power density at the imaging plane was 70 mW/cm², much lower than the safe exposure tolerance of 329 mW/cm² at 808 nm

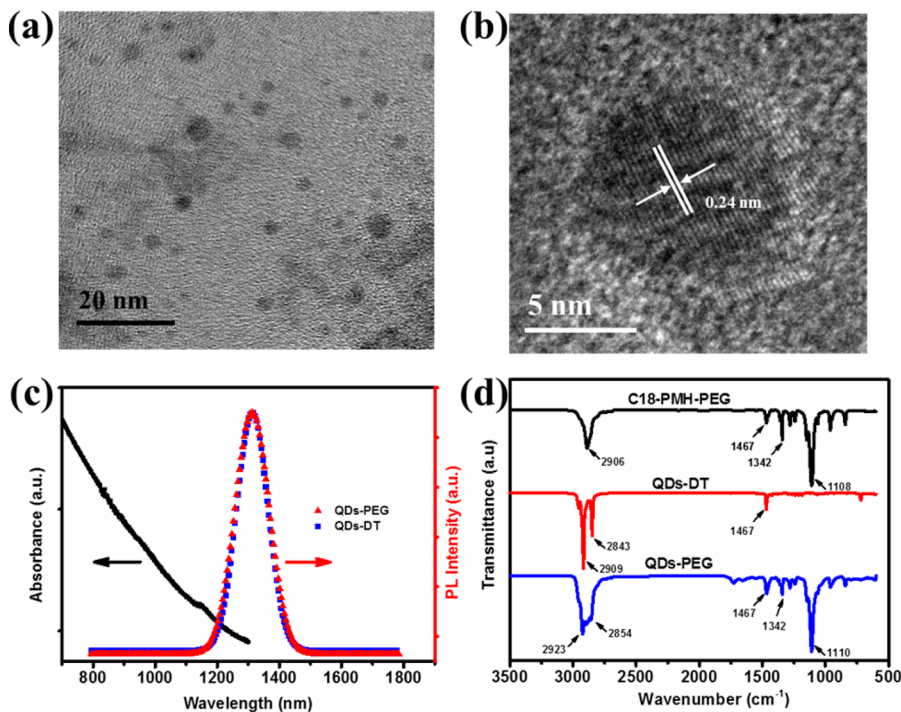


Figure 1. Characterization of Ag₂Se QDs-PEG. (a) TEM image. (b) HR-TEM image (interplanar spacing is indicated by white arrows). (c) Absorption spectrum of Ag₂Se QDs-PEG and photoluminescence emission spectrum of Ag₂Se QDs-DT and Ag₂Se QDs-PEG. (d) IR spectrum of C18-PMH-PEG, Ag₂Se QDs-DT, and Ag₂Se QDs-PEG. Wavelengths of functional groups are indicated by the arrows.

provided by the International Commission on Nonionizing Radiation Protection. The emitted light from the animal was filtered through two long-pass filters (900 and 1000 nm, Thorlabs) coupled with the InGaAs camera. The camera exposure time was set as 50 ms.

2.7. Serum Biochemistry Assays and Pathology Investigations. For serum biochemistry assays, blood samples (800 μ L of each) were collected from mice at 7 and 28 d after the intravenous injection with Ag₂Se QDs-PEG or saline. Serum fraction was separated by centrifugation (3000 rpm, 10 min) and stored at -20 °C before analysis. The serum biochemistry analyses were performed by Deyi Diagnostics (Beijing, China).

Major organs (liver, spleen, lungs, and kidneys) of mice were harvested at 7 and 28 d after the injection of Ag₂Se QDs-PEG and saline. Pieces cut from each organ sample were fixed in 4% paraformaldehyde, embedded in paraffin, sectioned at 8 μ m thickness, and stained with hematoxylin and eosin (H&E). The slices were examined under a microscope.

2.8. Statistical Analysis. Statistical analysis was performed by Student *t* test with unknown and unequal variances. The statistical difference was considered significant when *p* value < 0.05. The data are expressed as mean \pm standard deviation (SD).

3. RESULTS

3.1. Characterization of Ag₂Se QDs-PEG. On the basis of Ag₂Se QDs-DT (detailed characterization of Ag₂Se QDs-DT is provided in Supporting Information), PEG-coated Ag₂Se QDs were prepared. According to the TEM observation (Figure 1a), the average diameter of Ag₂Se QDs-PEG is 5.0 \pm 0.8 nm, slightly larger than that of Ag₂Se QDs-DT (4.8 nm, Figure S1c). In addition, the hydrodynamic diameter of Ag₂Se QDs-PEG is around 29.6 \pm 5.1 nm (Figure S2a), much larger than that under TEM. The coating of 5000 MW PEG and slight aggregation might be the reasons for the size increase. Both Ag₂Se QDs-DT and Ag₂Se QDs-PEG belong to orthorhombic phase (β -Ag₂Se), which is confirmed by the HR-TEM investigations (Figure 1b and Figure S1b) and XRD (Figure

S3). Ag₂Se QDs containing both Ag and Se are also confirmed by high-resolution XPS of Ag_{3d} and Se_{3d} (Figure S4b and S4c). The lattice spacing (ca. 0.24 nm) of Ag₂Se is consistent with the distance between adjacent facets (013) of orthorhombic Ag₂Se. The photoluminescence spectrum (Figure 1c) shows an emission peak centered at 1311 nm, indicating that the fluorescence property of Ag₂Se QDs is stable during the PEG coating process. The negative charge of Ag₂Se QDs-PEG (-13.4 mV, Figure S2b) may come from the residual COO⁻ groups of amphiphilic polymer. However, the amount of COO⁻ groups should be small, since no infrared (IR) signal is present in the IR spectrum (Figure 1d). In detail, the peaks at 1110 and 1342 cm⁻¹ in Ag₂Se QDs-PEG correspond to the C=O stretching band and the CH₂/CH₃ plane vibration of C18-PMH-PEG. The peaks located at 2923 and 2853 cm⁻¹ are assigned to symmetric and asymmetric stretching vibrations of C-H.

The Ag/Se ratios of Ag₂Se QDs-DT and Ag₂Se QDs-PEG are 3.32 and 3.53, respectively. The deviation of intrinsic stoichiometry of Ag₂Se in the synthesis and modification process may come from the high binding ability of silver and thiol compounds.¹⁷ The existence of element S in Ag₂Se QDs is confirmed by the EDX and XPS measurements (Figure S1d and S4a).

3.2. Blood Clearance. After entering the blood circulation, Ag₂Se QDs-PEG moves along with the blood and is gradually cleared and accumulated in various tissues. On the basis of the Ag and Se concentrations in the blood at different time points postinjection, we calculated the pharmacokinetic parameters by fitting the data over 24 h with the one-compartment model. The simulated blood circulation curves and main parameters are shown in Figure 2. Ag₂Se QDs-PEG is cleared from the blood circulation quickly. The blood circulation half-life ($T_{1/2}$) of Ag₂Se QDs-PEG is 0.406 h based on Ag concentrations and

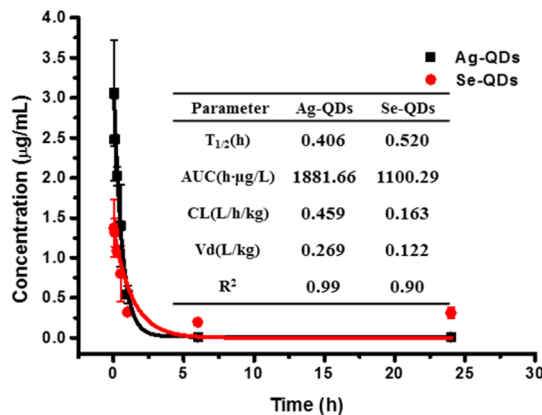


Figure 2. Blood concentrations and kinetics parameters of Ag and Se after intravenous injection of Ag_2Se QDs-PEG.

0.520 h based on Se concentrations. Apparently, Ag and Se of Ag_2Se QDs-PEG behave differently in blood. Beyond the different half-life times, bigger area under blood concentration–time profiles (AUC), faster clearance rate (CL), and higher apparent volume of distribution (V_d) are obtained based on Ag concentrations. These data indicate that Ag of Ag_2Se QDs-PEG is easier to be cleared out from blood circulation than Se.

Table 1 lists the Ag and Se concentrations in blood within 28 d after the injection of Ag_2Se QDs-PEG. In the first hour, the

Table 1. Concentration–Time profiles of Ag and Se in Blood after Intravenous Injection of Ag_2Se QDs-PEG

time	Ag (ng/mL)	Se (ng/mL)
2 min	3210.15 ± 352.50	1372.56 ± 362.07
5 min	2604.62 ± 541.43	1314.22 ± 175.20
15 min	2024.69 ± 124.09	1079.99 ± 24.44
30 min	1471.20 ± 538.14	801.35 ± 349.22
1 h	568.82 ± 114.70	321.96 ± 27.43
6 h	7.95 ± 0.23	195.56 ± 33.50
1 d	9.25 ± 2.27	310.71 ± 67.52
7 d	ND ^a	868.40 ± 123.08
14 d	ND	814.13 ± 112.35
28 d	ND	ND

^aND means undetectable.

concentration of Ag is much higher than that of Se. After that, the concentration of Ag drops quickly and is undetectable at 6 h. As for Se, its concentration continuously drops in the first 6 h. Then the concentration increases to 864.4 ng/mL at day 7 and keeps until day 14. At day 28, the Se concentration goes back to the control level.

3.3. Biodistribution. The Ag and Se contents in organs were simultaneously measured by using ICP-MS (Tables S1 and S2). Biodistribution profiles of Ag_2Se QDs-PEG are shown in Figure 3. Similar to the blood concentration results, Ag and Se show different distribution patterns. Liver is the major accumulation organ of both Ag and Se. Around 40% ID of Ag and 60% ID of Se distribute in liver after Ag_2Se QDs-PEG enters the body. The Ag and Se contents reach the maximum of 77.7% ID and 109.7% ID at 6 h, respectively. At day 28, around 2.5% ID of Ag and 15.6% ID of Se still remain there. Besides the liver, the spleen is also an accumulation organ of Ag. At 15 min after injection, 7% ID of Ag accumulates in the spleen, followed with 2.6% ID of Ag deposits in lungs. Along with the exposure time, the Ag content in the spleen keeps relatively stable (5.8–7.6% ID) within 1 d after injection. Then Ag is gradually cleared out from the spleen and drops to 1.0% ID at day 7. A similar change trend is found in the lungs. At day 28, the Ag contents in both the spleen and the lungs drop to 0.80% ID and those in the blood, heart, kidneys, and brain are hard to be detected, suggesting that Ag released from Ag_2Se QDs-PEG can be expelled from the body totally.

In addition to the liver, high Se accumulation is found in the spleen and kidneys. The Se content in the kidneys displays an increase trend from 3.6% ID to 12.5% ID during the first 14 d and then drops to 5.4% ID at day 28. Near 10% ID of Se accumulates in the spleen within 1 day postexposure and drops 1.8% ID at day 7. At day 28, the content value increases to 7.3% ID. No overt Se is found in the heart, lungs, and brain.

Taking advantage of the NIR fluorescence of Ag_2Se QDs-PEG, the distribution of Ag_2Se QDs-PEG in nude mice was assessed using noninvasive fluorescence imaging too. The fluorescence background of mice in the NIR II region is undetectable (Figure 4a). Once Ag_2Se QDs-PEG is intravenously injected to mice, the NIR II fluorescence is clearly observed in the superficial vasculature, and the intensity in abdomen increases to maximum at 15 min. The signals from the liver, bone, and spleen are strong. The fluorescence also seems to emerge on the position of the bladder, suggesting that

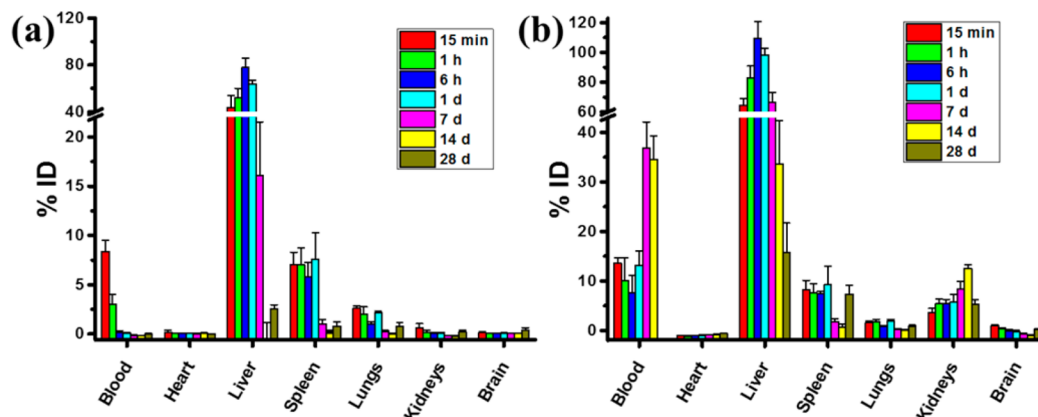


Figure 3. Distribution of Ag (a) and Se (b) in mouse organs after injection of Ag_2Se QDs-PEG. Mean values of the corresponding control were deducted as the baseline. All data are represented as the mean \pm SD ($n = 5$).

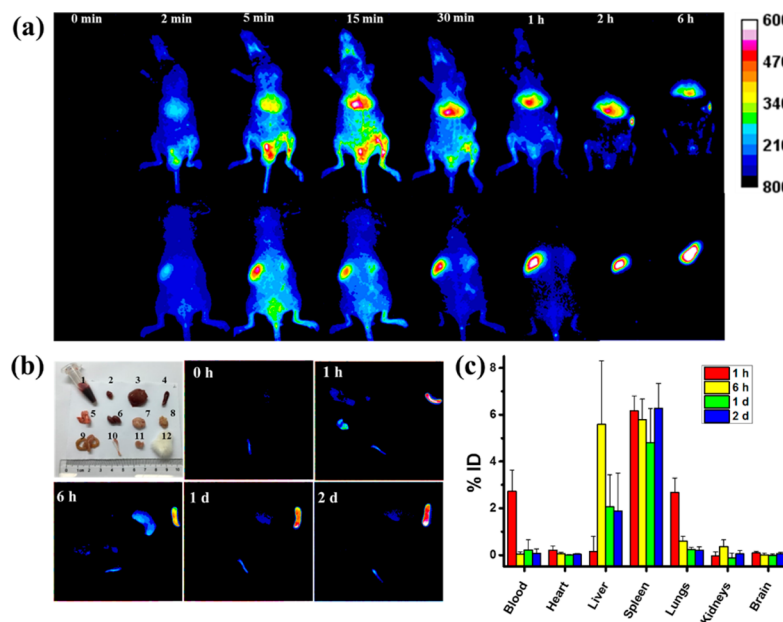


Figure 4. (a) In vivo fluorescence imaging of Ag_2Se QDs-PEG in nude mice within 6 h after intravenous injection. (Top row) Abdomen imaging; (bottom row) backside imaging. The contrast is set between 8000 and 60 000. (b) Representative ex vivo fluorescence images of Ag_2Se QDs-PEG in tissues after intravenous injection. Digital photos of tissues: 1, blood; 2, heart; 3, liver; 4, spleen; 5, lungs; 6, kidneys; 7, brain; 8, stomach; 9, intestine; 10, bone; 11, muscle; 12, skin with fur. (c) Distribution of Ag_2Se QDs-PEG in mice based on the fluorescence intensity (% ID) of tissues in (b) ($n = 4$).

Ag_2Se QDs-PEG is excreted through the urine pathway. Thirty minutes later, the signal in the vasculature begins to attenuate and almost disappears at 2 h. The fluorescence images confirm that Ag_2Se QDs-PEG tends to accumulate largely in the liver and spleen and is hard to be cleared out.

The distribution obtained by the fluorescence imaging was further confirmed by the ex vivo imaging of organs after animals were sacrificed at 1–48 h postexposure. As shown in Figure 4b, the strong fluorescence signal is clearly observed in the liver, lungs, spleen, and bone. The semiquantitative histogram based on fluorescence intensity-area integration is displayed in Figure 4c. About 5% ID of Ag_2Se QDs-PEG is found in the spleen, and the spleen uptake keeps constant during 48 h. Ag_2Se QDs-PEG deposits first in the blood, liver, and lungs around 3–5% ID, and the accumulation levels subsequently decrease along with the time. The different distribution data between element measurements and fluorescence intensities indicate that a majority of Ag_2Se QDs-PEG degrades and hence loses fluorescence in the liver. In addition, in the control group, all organs do not have NIR II background except bone (Figure S5b). Therefore, the high fluorescence intensity of bone does not come from Ag_2Se QDs-PEG but bone per se.

3.4. Biotransformation in Vivo and in Vitro. The different blood kinetics and distribution patterns of Ag and Se in vivo show that the two constituent elements Ag and Se in Ag_2Se QDs-PEG have different chemical fates in vivo, which could be indicated by the changed Ag/Se ratios in organs. The Ag/Se ratios in the four main accumulation organs were calculated to reveal the chemical change of Ag_2Se QDs-PEG (Table 2).

At 15 min, the Ag/Se ratios in four organs are approximately 3, which is consistent with the pristine molar ratio in Ag_2Se QDs-PEG. Along with time elapse, the ratios in all organs decrease, demonstrating the transformation of the original Ag_2Se QDs-PEG. Among four organs, the stability of Ag_2Se

Table 2. Molar Ratios of Ag/Se in Organs at Different Time Points Postexposure to Ag_2Se QDs-PEG

time	liver	spleen	lungs	kidneys
15 min	2.67 ± 0.48	3.09 ± 0.22	2.52 ± 0.60	3.37 ± 0.72
1 h	2.28 ± 0.35	3.40 ± 0.21	2.41 ± 0.37	2.95 ± 0.55
6 h	2.23 ± 0.56	3.36 ± 0.46	1.76 ± 0.11	3.23 ± 0.48
1 d	2.45 ± 0.05	3.16 ± 0.08	2.01 ± 0.27	1.87 ± 0.65
7 d	1.09 ± 0.26	2.89 ± 0.46	0.50 ± 0.29	0.07 ± 0.05
14 d	0.34 ± 0.29	1.67 ± 0.67	0.11 ± 0.08	0.02 ± 0.01
28 d	0.34 ± 0.11	0.45 ± 0.33	1.18 ± 0.51	0.18 ± 0.10

QDs-PEG in the spleen is the highest, while that in lungs is the worst. The Ag/Se ratio in the spleen keeps at around 3 at day 7. At the same time point, the ratios drop to 1.1 in the liver and 0.5 in the lungs. At day 28, the ratios drop to much lower values, indicating the serious collapse of Ag_2Se QDs-PEG.

To address the chemical change of Ag_2Se QDs-PEG in vivo more clearly, we tested the stability of Ag_2Se QDs-PEG in vitro. The first evaluation was performed in the SBF, which consists of ions with concentrations equal to those of the human plasma and is often used to evaluate the drug release from drug delivery systems.¹⁸ Figure 5 shows that Ag_2Se QDs-PEG is relatively stable in SBF. In the first hour, decomposition of Ag_2Se QDs-PEG increases quickly and then reaches a plateau. Less than 1% of Ag and Se decompose from Ag_2Se QDs-PEG, and the Ag/Se ratio keeps constant when the decomposition reaches the maximum. According to the composition of the SBF system, the remains in the dialysis bag are Ag_2Se QDs. The decomposition of Ag_2Se QDs-PEG is more significant in FBS, though the degradation trend is the same as that in SBF. At 1 h, 3.4% of Ag and 4.1% of Se are released from Ag_2Se QDs-PEG. The decomposition continues with a much slower speed thereafter. At day 3, 4.2% of Ag and 4.9% of Se are released from Ag_2Se QDs-PEG. Considering there are a lot of proteins in FBS, part of Ag and Se released from Ag_2Se QDs may bind

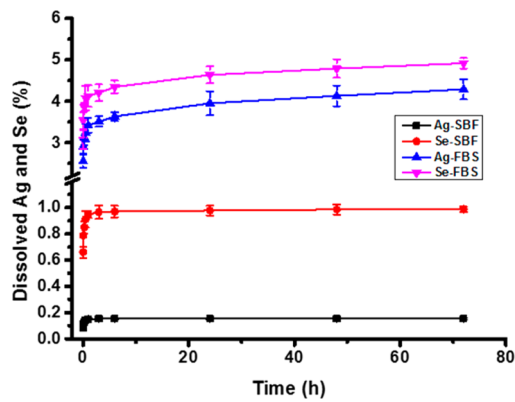


Figure 5. Stability of Ag_2Se QDs-PEG in SBF and FBS for 72 h.

to proteins and then remain in the dialysis bag. Therefore, the real decomposition of Ag_2Se QDs-PEG in FBS is higher than that we measured.

The state of Ag_2Se QDs-PEG remaining in the dialysis bag was checked, too. First, their fluorescence property maintains as the initial Ag_2Se QDs-PEG (Figure S6d). Second, the Ag/Se ratios (3.58 for SBF and 3.73 for FBS) are very similar to the initial Ag_2Se QDs-PEG (3.53). These indicate the remains in bags are Ag_2Se QDs. However, the average size of the QDs treated with FBS decreases to 3.4 ± 0.9 nm (Figure S6a and c), while that of the Ag_2Se QDs treated with SBF keeps unchanged (5.1 ± 0.9 nm, Figure S6b and S6c), which are consistent well with the decomposition of Ag_2Se QDs-PEG that happened in FBS.

3.5. Excretion of Ag_2Se QDs-PEG. The excreta samples of Ag_2Se QDs-PEG from mice were collected daily and analyzed to reveal the possible excretion pathways. As shown in Figure 6, Ag is detected in both urine and feces. During the periods of days 6–8 and days 20–22, distinguishable Ag is excreted from urine. In feces, the continual excretion of Ag is detected along with the time elapse. At day 28, the total excretion percentages of Ag through urine and feces are 12.7% ID and 14.5% ID, respectively. Nevertheless, no remarkable Se of Ag_2Se QDs-PEG can be found in excreta (Figure 6a and 6b). This further supports that most of Se is retained in the body and hard to be excreted from tissues.

3.6. Toxicity. For safe applications in the future, it is vital to understand the potential toxicity of Ag_2Se QDs-PEG. The toxicity of Ag_2Se QDs-PEG in mice over 28 d was investigated at a high dose of $8 \mu\text{mol}/\text{kg}$ by a single intravenous injection. Over the 28 d observation period, no animal death occurs and the body weights of the control group and the Ag_2Se QDs-PEG group have similar increasing trends (Figure 7a). At days 7 and 28, the organ indexes are calculated to reflect the organ damage induced by Ag_2Se QDs-PEG (Figure 7b). No significantly abnormal organ index is observed, except the decreased organ index of liver at day 28, suggesting potential damage to the liver.

Serum biochemistry plays an important role in evaluating organ functions. A series of biochemical parameters, including total protein (TP, g/L), albumin (ALB, g/L), globulin (GLB, g/L), alanine aminotransferase (ALT, U/L), alkaline phosphatase (ALP, U/L), aspartate aminotransferase (AST, U/L), creatinine (CR, μM), total bilirubin (TBIL, μM), albumin/globulin (A/G), blood urea nitrogen (BUN, mmol/L), glucose

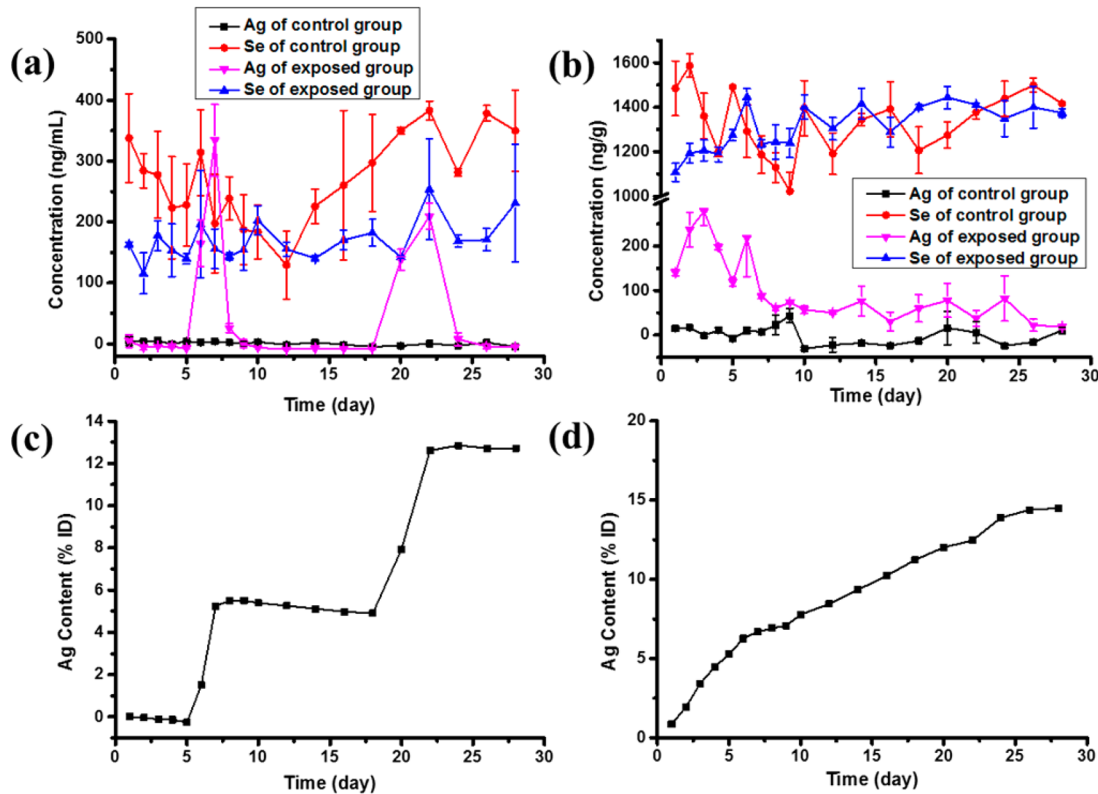


Figure 6. Excretion of Ag_2Se QDs-PEG from mice ($n = 4$). (a) Contents of Ag and Se in urine; (b) contents of Ag and Se in feces; (c) integrated excretion of Ag from urine; (d) integrated excretion of Ag from feces.

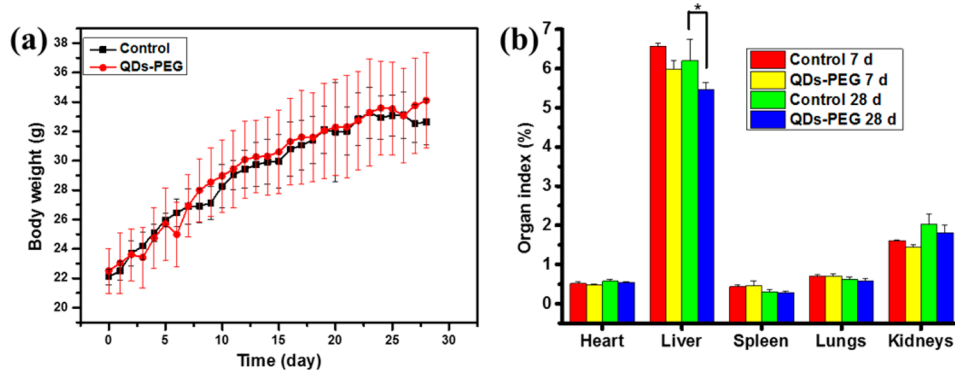


Figure 7. Body weigh changes (a) and organ indexes (b) of mice at days 7 and 28 after intravenously injection with Ag₂Se QDs-PEG at a dose of 8 μmol/kg b.w. ($n = 5$).

Table 3. Serum Biochemical Parameters at Days 7 and 28 Postexposure to Ag₂Se QDs-PEG at a Dose of 8 μmol/kg b.w. ($n = 5$)

parameter	day 7		day 28	
	control	QDs-PEG	control	QDs-PEG
CR (μmol/L)	6.36 ± 4.40	5.72 ± 1.90	1.43 ± 1.13	3.57 ± 1.62 ^a
TBIL (μmol/L)	0.68 ± 0.48	0.30 ± 0.37	1.51 ± 1.08	0.67 ± 0.30
TP (g/L)	50.10 ± 0.93	52.78 ± 2.35	51.69 ± 3.01	50.77 ± 4.23
ALB (g/L)	30.73 ± 0.84	32.82 ± 1.01	32.24 ± 1.70	31.18 ± 2.18
GLB (g/L)	19.38 ± 0.53	19.96 ± 1.71	19.44 ± 1.39	19.58 ± 2.22
A/G	1.59 ± 0.06	1.65 ± 0.14	1.66 ± 0.06	1.60 ± 0.10
ALT (U/L)	40.60 ± 9.43	33.76 ± 9.72	59.57 ± 15.01	53.80 ± 15.48
ALP (U/L)	153.78 ± 24.17	123.70 ± 18.70	123.76 ± 26.45	124.05 ± 27.62
BUN (mmol/L)	7.94 ± 1.71	9.61 ± 1.28	10.11 ± 1.46	9.32 ± 0.97
UA (μmol/L)	105.20 ± 27.45	99.64 ± 18.47	123.37 ± 43.58	203.93 ± 67.32 ^a
GLU (mmol/L)	10.39 ± 1.12	8.78 ± 1.34	6.99 ± 1.33	8.06 ± 1.28
AST (U/L)	152.58 ± 21.48	137.90 ± 43.41	189.57 ± 50.76	175.33 ± 74.79
LDH (U/L)	989.31 ± 169.02	881.34 ± 154.31	785.31 ± 200.87	1236.36 ± 559.47

^a $p < 0.05$ comparing with the control group.

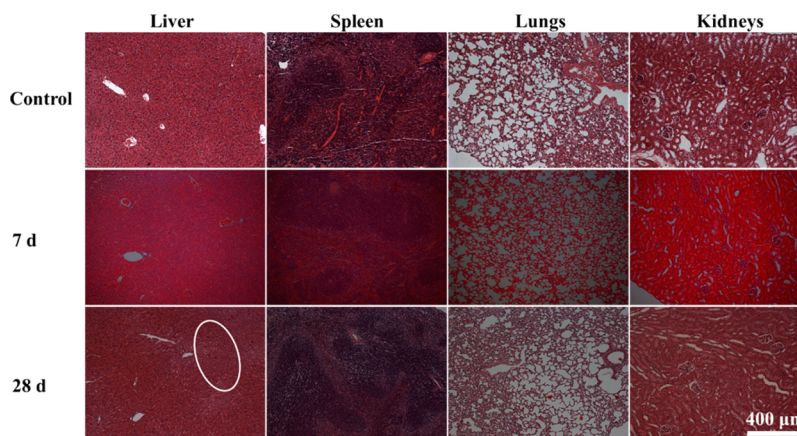


Figure 8. Representative H&E stained images of major organs at days 7 and 28 after injection of Ag₂Se QDs-PEG and saline (the control group). The slight edema and necrosis in the liver at day 28 are indicated by the circle. All images are at the same magnification, and the scale bar is given at the right bottom.

(GLU, mmol/L), uric acid (UA, mM), and lactate dehydrogenase (LDH, U/L), were all measured (Table 3). At day 7, all these parameters keep in normal ranges. At day 28, the CR and UA levels increase markedly, showing the adverse effects on the renal functions.

To further assess the toxicity of Ag₂Se QDs-PEG to mice, pathological section observation of the main organs including the liver, spleen, lungs, and kidneys was made. As shown in

Figure 8, the liver is normal at day 7, but slight edema and necrosis are found in the liver at day 28, which are consistent with the suppressed organ index of the liver. The other organs are normal at days 7 and 28.

4. DISCUSSION

NIR II QDs have gained considerable attention due to their potential applications in bioimaging, photoelectronic device,

and biosensing.⁸ In light of the advantageous spectral region and less metallic toxicity of Ag₂Se QDs, they have been considered as promising imaging agents.^{9–11} According to our findings, we infer that Ag₂Se QDs are suitable for biomedical imaging *in vivo* from the biosafety perspective.

4.1. Blood Clearance. Blood clearance of Ag₂Se QDs-PEG displays how fast Ag₂Se QDs-PEG leaves the bloodstream and enters organs. Ag₂Se QDs-PEG has a short blood half-life of 0.4 h according to the measurements of Ag, while Se has different pharmacokinetics parameters compared with Ag. It is believed that PEGylation could prolong the blood circulation of nanoparticles.¹⁹ However, in this study, Ag₂Se QDs-PEG is quickly cleared out in blood despite the existence of PEG, which may be related to the small size of Ag₂Se QDs, even coated with PEG, compared with other nanoparticles. Similarly, Meng et al. reported that PEGylated small QDs were cleared from blood fast.²⁰ In this study, most of Ag₂Se QDs are captured by the liver in a short time, which results in the fast clearance of Ag₂Se QDs in the blood. In fact, the liver is capable specifically to capture and eliminate nanoparticles larger than 10–20 nm and smaller than 100 nm in hydrodynamic diameter.²¹ In addition, no Ag₂Se QD was collected in urine in the first few days in this study, indicating renal clearance is not a main excretion route for Ag₂Se QDs. We attribute the fast clearance of the Ag₂Se QDs from the blood to liver uptake instead of renal clearance.

The increase of Se concentration in the blood at days 7 and 14 may be ascribed to the redistribution of selenium through the metabolism network. Ag₂Se QDs degraded significantly at day 7 after injection, especially in the liver, releasing inorganic selenium, which can be further metabolized into the comprehensive selenium biochemical metabolism pathways. The liver, where the most of Ag₂Se QDs retained, is the foremost organ for Se metabolism, for synthesizing most of the Se proteins, and for regulating the excretion of Se metabolites. The Se proteins produced in the liver are released into the blood stream and are responsible for the distribution of Se to the other organs.²²

4.2. Biodistribution. In previous studies, fluorescence imaging has been used to quantify QDs in blood and organs *in vivo*.^{20,23} However, the fluorescence intensity of QDs in the body has marked interference with the high and variable background fluorescence from blood and tissues. Moreover, the fluorescence is susceptible to many factors such as surface chemistry, rearrangement of surface ligands, photoenhanced oxidation, and solvent effects.²⁴ Any of these parameters may potentially cause large deviations in fluorescence measurements. ICP-MS is a sensitive method to detect most elements with high accuracy and low detection limit, so we adopted it to measure the biodistribution of Ag₂Se QDs-PEG in mice. Of course, in order to view directly the location of Ag₂Se QDs-PEG in animals, NIR-II fluorescence imaging as a supplementary approach were also used.

Results of both NIR-II fluorescence imaging and ICP-MS show that the liver, spleen, lungs, and kidneys are the main accumulation organs of Ag₂Se QDs-PEG. The liver and spleen are the primary organs of the reticuloendothelial system (RES), and the hepatic and splenic accumulation of Ag₂Se QDs-PEG resulted from the uptake of the phagocytic cells.²⁵ In addition, the size of the Ag₂Se QDs-PEG in our study is smaller than the pore size of liver fenestrata (ca. 100 nm), which may also enhance the liver uptake. The body burden of Ag₂Se QDs-PEG in the lungs may be due to the aggregation of Ag₂Se QDs-PEG,

which is mainly induced by the proteins in blood. The large aggregates often cause transient embolism in the lung capillaries followed by redistribution to the liver.²⁶ The accumulation in kidneys might imply renal excretion of Ag₂Se QDs-PEG.

4.3. Transformation and Metabolism. To date, some previous studies have addressed the chemical fate and decomposition of Cd-contained QDs in mice. For example, blue-shifted emission peaks of CdSe QDs in the liver, spleen, and lymph nodes of mice were observed after 2 year metabolism, reflecting the breakdown of CdSe QDs in these organs.²⁷ CdSe QDs decomposed, and their fluorescence was quenched in *Caenorhabditis elegans* at 24 h postexposure.²⁸ The decomposition of CdTe was reflected by the different blood kinetics and biodistribution behaviors between Cd and Te in mice over 28 d.^{29,30} In this study, we observed the different behaviors of Ag and Se, implying the biotransformation of Ag₂Se QDs-PEG. Ag accumulates primarily in the liver and spleen, while high levels of Se persist in the blood, liver, and kidneys. In a period of 1 d, the distribution of Se is similar to that of Ag. However, compared to Ag, Se displays different accumulations in organs thereafter and an increase trend of Se emerges in the blood and kidneys. At day 28, the residual Se in the body is much more than Ag, showing that Se is much harder than Ag to be cleared out of body. This phenomenon is well understood because the heavy metal Ag is xenobiotic, and finally should be excluded from the body. Whereas Se, an essential trace element, could be transferred into the Se-contained biomolecules after decomposition of Ag₂Se QDs-PEG, eventually the Se element of Ag₂Se QDs-PEG enters into the normal metabolism network. This perspective is compatible with the different excretion rate of Ag and Se.

The decomposition process of Ag₂Se QDs-PEG is dynamic, which depends on the accumulation time and organs to a great extent. Generally, the longer time Ag₂Se QDs-PEG lingers in the body, the higher possibility of decomposition occurs. We simultaneously calculated the Ag/Se ratios in tissues over 28 d showing the *in vivo* decomposition (Table 2). As a whole, the ratios do not change much within 1 d after exposure but significantly decrease at day 7, which implies that the decomposition degree of Ag₂Se QDs-PEG is anabolic with time. This hypothesis is further confirmed by the dissolution experiment of Ag₂Se QDs-PEG in the SBF and FBS, in which the percentages of dissolved Ag and Se increase quickly with increasing exposure time in fluids. The fact that the longer lingering time of Ag₂Se QDs-PEG in body increases the risk of metal ion leakage has been verified in our work.

Beyond the time-dependent decomposition, the ratio changes are different in different tissues, suggesting that the decomposition of Ag₂Se QDs-PEG is organ dependent. The Ag/Se ratios are relatively constant in the spleen. However, sharp decreases of the ratios are observed in the liver, lungs, and kidneys after 1 d. Consistently, the *ex vivo* fluorescence imaging results clearly show that high fluorescence intensity is observed in the spleen all the time, while the brightness in the liver fades out significantly with time. The great fluorescence quenching in the liver may be partly attributed to the localized surface defects in the short term.³¹ The different decomposition rates of Ag₂Se QDs in organs are closely related to the intrinsic roles these organs play. The liver is the main organ of metabolic clearance of most drugs and xenobiotics. It is known that there are a large number of phase I and phase II enzymes in the liver, for example, monooxygenase, transferases, esterases, and epoxide hydrolase. As the largest immune organ in the lymphatic

system, the spleen contains a lot of lymphocytes and macrophages; however, it lacks various enzymes. Parts of Ag₂Se QDs deposited in the liver are more likely to be dissolved or biodegraded by enzymatic catalysis, for instance, in the case of magnetic iron oxide nanoparticles and single-walled carbon nanotubes.^{32,33} Despite the Ag₂Se QDs being trapped in the spleen by monocyte macrophage uptake, the spleen is incapable to provide enough biologically active enzymes or chemically active compounds for digesting these xenobiotic Ag₂Se QDs. Thus, the degree and speed of decomposition of the Ag₂Se QDs in the liver is much higher than that in the spleen.

The stability experiments of Ag₂Se QDs-PEG in SBF and FBS also show that the biomolecules accelerate the dissolution of Ag₂Se QDs-PEG. However, compared with the *in vivo* decomposition data, the dissolution in SBF or FBS is much lower. It implies that direct dissolution is not the main reason for biotransformation. On the other hand, the different decomposition behaviors in different organs show that the biochemical environment in a proper organ is a determining factor for transformation. As mentioned above, the liver is the main organ of metabolic clearance of most drugs and xenobiotics. Lysosomal-associated degradation is a dominant pathway for Kupffer cells (KCs, liver macrophage cells) to clear xenobiotics. When nanomaterials are trapped in the lysosome of KC, the acidic microenvironment of lysosome and the large number of acid hydrolase enzymes may cause dissolution or enzymatic decomposition of nanomaterials.³⁴ Lunov et al. demonstrated other metal-based nanoparticles could be entrapped in lysosomal vesicles and dissolved or degraded by lysosomal α-glucosidase.³² Furthermore, the latest findings showed that after incubation with human hepatocellular carcinoma cells (HepG2), CdSe/ZnS QDs leaked out cadmium ions, which further bound to metallothioneins, a kind of small, sulphydryl-rich, metal-binding protein.³⁵

On the basis of the tissue-specific and time-dependent decomposition, we propose a possible process about the chemical change of Ag₂Se QDs-PEG in the liver: In the initial stage, fluorescence of Ag₂Se QDs-PEG is quickly quenched because of the erosion of surface structure, which might be caused by the interaction with proteins and/or acidic microenvironment. In later days, Ag₂Se QDs-PEG gradually decomposes to release ions, and the chemical constitution of Ag₂Se QDs-PEG alters, finally leading to the change of the Ag/Se ratio. Similar to Cd ions, Ag ions could bind with proteins such as metallothioneins, which might be subsequently cleared out of body. The detailed process of how Ag₂Se QDs-PEG interacts with biomolecules and gets metabolized *in vivo* still needs to be investigated in the future.

4.4. Excretion. Elucidation of the excretion mechanism and pathways is important in potential applications and the toxicity assessment of Ag₂Se QDs-PEG. There are some researches focused on the excretion of QDs and related influencing factors.^{21,36,37} The clearance of intravenously injected QDs can proceed through two ways: One is from the liver into feces through the biliary pathway; another is renal excretion, from the kidneys into urine through the bladder pathway. Our results show that Ag of Ag₂Se QDs-PEG can be cleared out through both renal and fecal excretions. However, the other constituent element Se is in a low concentration level in excreta compared with the control group.

Choi et al. reported that the hydrodynamic diameter of nanoparticles was a critical parameter to determine whether

nanoparticles could be excreted efficiently through urine, and nanoparticles with a hydrodynamic diameter less than 5.5 nm could result in rapid clearance through the kidneys.²¹ The hydrodynamic diameter of Ag₂Se QDs-PEG is around 29.6 nm, larger than the threshold value, meaning Ag₂Se QDs-PEG cannot be directly excreted through urine. It is also confirmed by the fact that no Ag is detected in urine in the first 5 d after injection. During the period of days 6–8 and days 20–22, a remarkable amount of Ag is found in urine, which should be due to the decomposition-generated Ag ions. Interestingly, the concentration of Ag in the kidneys decreases from 218.31 ng/g at day 1 to 59.69 ng/g at day 7 (Table S2), which corresponds to excretion through urine in the period of days 6–8. The excretion at days 20–22 and increase of concentration in the kidneys from day 14 to day 28 may come from the Ag redistribution in the whole body.

4.5. Toxicity. The data of body weight, organ index, serum biochemistry, and pathological examination show that Ag₂Se QDs-PEG at day 7 postexposure does not induce any significant adverse effect *in vivo*. The organ index of the liver for the Ag₂Se QDs-PEG group at day 28 is lower than that for the control group, which means atrophy of the liver. Ag₂Se QDs-PEG shows nonspecific uptake in the RES organs, mainly accumulating in the spleen and liver, and subsequently decomposes to release metal ions, which are judged as the main cause of nanotoxicity. In Figure 8, the slight edema and necrosis of the liver induced by Ag₂Se QDs-PEG correspond to the relevant decrease of the liver index. It gives us awareness that long-term high-dose exposure to Ag₂Se QDs-PEG may result in tiny hepatotoxicity after a single intravenous injection.

Some papers reported the hepatotoxicity induced by silver nanoparticles.^{38,39} Excessive accumulation/deposition of silver nanoparticles in the liver caused certain adverse effects including marked pathological changes in liver morphology, bile duct hyperplasia, inflammatory cell infiltration, generation of excessive reactive oxygen species, DNA damage, and liver enzyme activity changes and finally led to apoptosis and necrosis.³⁸ The latest study on ionic silver showed that the ionic silver (silver acetate) was more cytotoxic to HepG2 cells compared with the silver nanoparticles.⁴⁰ However, the influence of chemical species of Ag on the hepatic toxicity is unclear in these studies. Although slight liver toxicity is observed, it is really worth stating that the dose of Ag₂Se QDs-PEG (8 μmol/kg) is much higher than that in previous works of CdSe QDs and analogues (from several pmol/kg to several μmol/kg).^{26,41} This indicates that Cd-free Ag₂Se QDs-PEG possesses less toxicity and better biocompatibility than the traditional cadmium-based QDs.

4.6. Instability Caused by Biotransformation. In spite of the ultralow solubility product constant (K_{sp} (Ag₂Se) = 2.0×10^{-64}), decomposition of Ag₂Se QDs-PEG under the complex and dynamic biological system is observed. The *in vivo* instability of Ag₂Se QDs-PEG may impede the long-term imaging applications, because the fluorescence of Ag₂Se QDs-PEG will be attenuated with time. PEG, a macromolecule polymer, provides Ag₂Se cores a stealth coat, makes Ag₂Se cores water soluble, and protects Ag₂Se cores against interaction with proteins. However, it is not an effective coating shell to avert biotransformation and maintain the original integrity of Ag₂Se cores *in vivo*.^{31,42}

In order to realize the potential applications of Ag₂Se QDs in the future, it is necessary to greatly improve its stability against the biotransformation *in vivo*. Traditionally, the widely used

QDs, e.g., CdSe, CdTe, or CdS, are always coated with inorganic shell ZnS, CdS, or silica to enhance the fluorescence stability and oxidation resistance.⁴³ Therefore, developing Ag₂Se QDs into a similar core–shell structure might be a hopeful way to solve its biotransformation problem. Besides the shell coating, surface modification ligands may also provide Ag₂Se cores the second protection layer against the external environment. Thus, enhancing the affinity between the ligands and the shell and increasing the density of ligands on the surface would retard the decomposition of the inorganic nanoparticle cores.⁴⁴ In summary, finding suitable shells and ligands for Ag₂Se QDs to improve the *in vivo* stability is a key step to push this novel NIR II QDs up to clinical applications.

5. CONCLUSIONS

In summary, the blood clearance, distribution, transformation, excretion, and toxicity of Ag₂Se QDs-PEG are systematically investigated in mice after a single intravenous injection. Ag₂Se QDs-PEG prefers to accumulate in the spleen and liver but is almost transformed and/or cleared within 1 d. Biotransformation of Ag₂Se QDs depends on the organs deposited and the length of accumulation period. Interestingly, Ag released from Ag₂Se QDs-PEG is excreted through both feces and urine, whereas essential element Se is excreted hardly. Ag₂Se QDs-PEG only shows slight toxicity to liver at day 28 postexposure, even at a high dose of 8 μmol/kg b.w., while no other hazard is found during the 28 d observation. Our results collectively indicate that Ag₂Se QDs-PEG is of low toxicity and will inspire the developments and applications of Ag₂Se QDs with high performance and good biosafety.

■ ASSOCIATED CONTENT

Supporting Information

The Supporting Information is available free of charge on the ACS Publications website at DOI: [10.1021/acsami.6b05057](https://doi.org/10.1021/acsami.6b05057).

Additional synthesis, characterization of Ag₂Se QDs-DT and Ag₂Se QDs-PEG, characterization of Ag₂Se QDs-PEG in dialysis bags after dialysis in SBF and FBS, and extra distribution data ([PDF](#))

■ AUTHOR INFORMATION

Corresponding Authors

*Tel.: 86-21-66138026, fax: 86-21-66135275, e-mail: hwang@shu.edu.cn.

*Tel.: 86-10-62757196, fax: 86-10-62754127, e-mail: yliu@pku.edu.cn.

Notes

The authors declare no competing financial interest.

■ ACKNOWLEDGMENTS

We thank the National Basic Research Program of China (Nos. 2016YFA0201600 and 2011CB933402), the Chinese Natural Science Foundation (No. 31571024), and the Top-notch Young Talents Program of China for financial support.

■ REFERENCES

- (1) Michalet, X.; Pinaud, F. F.; Bentolila, L. A.; Tsay, J. M.; Doose, S.; Li, J. J.; Sundaresan, G.; Wu, A. M.; Gambhir, S. S.; Weiss, S. Quantum Dots for Live Cells, *in vivo* Imaging, and Diagnostics. *Science* **2005**, *307*, 538–544.
- (2) Medintz, I. L.; Uyeda, H. T.; Goldman, E. R.; Mattoussi, H. Quantum Dot Bioconjugates for Imaging, Labelling and Sensing. *Nat. Mater.* **2005**, *4*, 435–446.
- (3) Zhou, J.; Yang, Y.; Zhang, C. Y. Toward Biocompatible Semiconductor Quantum Dots: From Biosynthesis and Bioconjugation to Biomedical Application. *Chem. Rev.* **2015**, *115*, 11669–11717.
- (4) Liu, S. L.; Wang, Z. G.; Zhang, Z. L.; Pang, D. W. Tracking Single Viruses Infecting Their Host Cells using Quantum Dots. *Chem. Soc. Rev.* **2016**, *45*, 1211–1224.
- (5) Hardman, R. A Toxicologic Review of Quantum Dots: Toxicity Depends on Physicochemical and Environmental Factors. *Environ. Health Perspect.* **2006**, *114*, 165–172.
- (6) Smith, A. M.; Duan, H.; Mohs, A. M.; Nie, S. Bioconjugated Quantum Dots for *in vivo* Molecular and Cellular Imaging. *Adv. Drug Delivery Rev.* **2008**, *60*, 1226–1240.
- (7) Cassette, E.; Helle, M.; Bezdetnaya, L.; Marchal, F.; Dubertret, B.; Pons, T. Design of New Quantum Dot Materials for Deep Tissue Infrared Imaging. *Adv. Drug Delivery Rev.* **2013**, *65*, 719–731.
- (8) Xu, S.; Cui, J.; Wang, L. Recent Developments of Low-Toxicity NIR II Quantum Dots for Sensing and Bioimaging. *TrAC, Trends Anal. Chem.* **2016**, *80*, 149–155.
- (9) Yarema, M.; Pichler, S.; Sytnyk, M.; Seyrkammer, R.; Lechner, R. T.; Fritz-Popovski, G.; Jarzab, D.; Szendrei, K.; Resel, R.; Korovyanko, O.; Loi, M. A.; Paris, O.; Hesser, G.; Heiss, W. Infrared Emitting and Photoconducting Colloidal Silver Chalcogenide Nanocrystal Quantum Dots from a Silylamine-Promoted Synthesis. *ACS Nano* **2011**, *5*, 3758–3765.
- (10) Gu, Y. P.; Cui, R.; Zhang, Z. L.; Xie, Z. X.; Pang, D. W. Ultrasmall Near-Infrared Ag₂Se Quantum Dots with Tunable Fluorescence for *in vivo* Imaging. *J. Am. Chem. Soc.* **2012**, *134*, 79–82.
- (11) Dong, B.; Li, C.; Chen, G.; Zhang, Y.; Zhang, Y.; Deng, M.; Wang, Q. Facile Synthesis of Highly Photoluminescent Ag₂Se Quantum Dots as a New Fluorescent Probe in the Second Near-Infrared Window for *in vivo* Imaging. *Chem. Mater.* **2013**, *25*, 2503–2509.
- (12) Lim, Y. T.; Kim, S.; Nakayama, A.; Stott, N. E.; Bawendi, M. G.; Frangioni, J. V. Selection of Quantum Dot Wavelengths for Biomedical Assays and Imaging. *Mol. Imaging* **2003**, *2*, 50–64.
- (13) Tan, L.; Wan, A.; Zhao, T.; Huang, R.; Li, H. Aqueous Synthesis of Multidentate Polymer-Capping Ag₂Se Quantum Dots with Bright Photoluminescence Tunable in a Second Near-Infrared Biological Window. *ACS Appl. Mater. Interfaces* **2014**, *6*, 6217–6222.
- (14) Tsoi, K. M.; Dai, Q.; Alman, B. A.; Chan, W. C. Are Quantum Dots Toxic? Exploring the Discrepancy between Cell Culture and Animal Studies. *Acc. Chem. Res.* **2013**, *46*, 662–671.
- (15) Kokubo, T.; Takadama, H. How Useful is SBF in Predicting *in vivo* Bone Bioactivity? *Biomaterials* **2006**, *27*, 2907–2915.
- (16) Wang, J.; Deng, X.; Yang, S.; Wang, H.; Zhao, Y.; Liu, Y. Rapid Translocation and Pharmacokinetics of Hydroxylated Single-Walled Carbon Nanotubes in Mice. *Nanotoxicology* **2008**, *2*, 28–32.
- (17) Shi, L. J.; Zhu, C. N.; He, H.; Zhu, D. L.; Zhang, Z. L.; Pang, D. W.; Tian, Z. Q. Near-Infrared Ag₂Se Quantum Dots with Distinct Absorption Features and High Fluorescence Quantum Yields. *RSC Adv.* **2016**, *6*, 38183–38186.
- (18) Marques, M. R.; Loebenberg, R.; Almukainzi, M. Simulated Biological Fluids with Possible Application in Dissolution Testing. *Dissolution Technol.* **2011**, *18*, 15–28.
- (19) Yang, S. T.; Fernando, K. A.; Liu, J. H.; Wang, J.; Sun, H. F.; Liu, Y.; Chen, M.; Huang, Y.; Wang, X.; Wang, H.; Sun, Y. P. Covalently PEGylated Carbon Nanotubes with Stealth Character *in vivo*. *Small* **2008**, *4*, 940–944.
- (20) Meng, X.; Qiang, L.; Wei, J. An Overview on the Pharmacokinetics of Quantum Dots. *Curr. Drug Metab.* **2013**, *14*, 820–831.
- (21) Choi, H. S.; Liu, W.; Misra, P.; Tanaka, E.; Zimmer, J. P.; Ipe, B. I.; Bawendi, M. G.; Frangioni, J. V. Renal Clearance of Quantum Dots. *Nat. Biotechnol.* **2007**, *25*, 1165–1170.
- (22) Roman, M.; Jitaru, P.; Barbante, C. Selenium Biochemistry and Its Role for Human Health. *Metallomics* **2014**, *6*, 25–54.

- (23) Pic, E.; Bezdetnaya, L.; Guillemin, F.; Marchal, F. Quantification Techniques and Biodistribution of Semiconductor Quantum Dots. *Anti-Cancer Agents Med. Chem.* **2009**, *9*, 295–303.
- (24) Chen, Z.; Chen, H.; Meng, H.; Xing, G.; Gao, X.; Sun, B.; Shi, X.; Yuan, H.; Zhang, C.; Liu, R.; Zhao, F.; Zhao, Y.; Fang, X. Bio-Distribution and Metabolic Paths of Silica Coated CdSeS Quantum Dots. *Toxicol. Appl. Pharmacol.* **2008**, *230*, 364–371.
- (25) Almeida, J. P. M.; Chen, A. L.; Foster, A.; Drezek, R. *In vivo* Biodistribution of Nanoparticles. *Nanomedicine* **2011**, *6*, 815–835.
- (26) Tang, Y.; Han, S.; Liu, H.; Chen, X.; Huang, L.; Li, X.; Zhang, J. The Role of Surface Chemistry in Determining *in vivo* Biodistribution and Toxicity of CdSe/ZnS Core–Shell Quantum Dots. *Biomaterials* **2013**, *34*, 8741–8755.
- (27) Fitzpatrick, J. A.; Andreko, S. K.; Ernst, L. A.; Waggoner, A. S.; Ballou, B.; Bruchez, M. P. Long-Term Persistence and Spectral Blue Shifting of Quantum Dots *in vivo*. *Nano Lett.* **2009**, *9*, 2736–2741.
- (28) Qu, Y.; Li, W.; Zhou, Y.; Liu, X.; Zhang, L.; Wang, L.; Li, Y. F.; Lida, A.; Tang, Z.; Zhao, Y.; Chai, Z.; Chen, C. Full Assessment of Fate and Physiological Behavior of Quantum Dots Utilizing *Caenorhabditis elegans* as a Model Organism. *Nano Lett.* **2011**, *11*, 3174–3183.
- (29) Han, Y.; Xie, G.; Sun, Z.; Mu, Y.; Han, S.; Xiao, Y.; Liu, N.; Wang, H.; Guo, C.; Shi, Z.; Li, Y.; Huang, P. Plasma Kinetics and Biodistribution of Water-Soluble CdTe Quantum Dots in Mice: A Comparison between Cd and Te. *J. Nanopart. Res.* **2011**, *13*, 5373–5380.
- (30) Liu, N.; Mu, Y.; Chen, Y.; Sun, H.; Han, S.; Wang, M.; Wang, H.; Li, Y.; Xu, Q.; Huang, P.; Sun, Z. Degradation of Aqueous Synthesized CdTe/ZnS Quantum Dots in Mice: Differential Blood Kinetics and Biodistribution of Cadmium and Tellurium. *Part. Fibre Toxicol.* **2013**, *10*, 37.
- (31) Mancini, M. C.; Kairdolf, B. A.; Smith, A. M.; Nie, S. Oxidative Quenching and Degradation of Polymer-Encapsulated Quantum Dots: New Insights into the Long-Term Fate and Toxicity of Nanocrystals *in vivo*. *J. Am. Chem. Soc.* **2008**, *130*, 10836–10837.
- (32) Lunov, O.; Syrovets, T.; Röcker, C.; Tron, K.; Nienhaus, G. U.; Rasche, V.; Mailänder, V.; Landfester, K.; Simmet, T. Lysosomal Degradation of the Carboxydextrans Shell of Coated Superparamagnetic Iron Oxide Nanoparticles and the Fate of Professional Phagocytes. *Biomaterials* **2010**, *31*, 9015–9022.
- (33) Kagan, V. E.; Konduru, N. V.; Feng, W.; Allen, B. L.; Conroy, J.; Volkov, Y.; Vlasova, I. I.; Belikova, N. A.; Yanamala, N.; Kapralov, A.; Tyurina, Y. Y.; Shi, J.; Kisin, E. R.; Murray, A. R.; Franks, J.; Stoltz, D.; Gou, P.; Klein-Seetharaman, J.; Fadeel, B.; Star, A.; Shvedova, A. A. Carbon Nanotubes Degraded by Neutrophil Myeloperoxidase Induce Less Pulmonary Inflammation. *Nat. Nanotechnol.* **2010**, *5*, 354–359.
- (34) Wang, B.; Feng, W.; Zhao, Y.; Chai, Z. Metallomics Insights for *in vivo* Studies of Metal Based Nanomaterials. *Metallomics* **2013**, *5*, 793–803.
- (35) Peng, L.; He, M.; Chen, B.; Qiao, Y.; Hu, B. Metallomics Study of CdSe/ZnS Quantum Dots in HepG2 Cells. *ACS Nano* **2015**, *9*, 10324–10334.
- (36) Schipper, M. L.; Iyer, G.; Koh, A. L.; Cheng, Z.; Ebenstein, Y.; Aharoni, A.; Keren, S.; Bentolila, L. A.; Li, J.; Rao, J.; Chen, X.; Banin, U.; Wu, A. M.; Sinclair, R.; Weiss, S.; Gambhir, S. S. Particle Size, Surface Coating, and PEGylation Influence the Biodistribution of Quantum Dots in Living Mice. *Small* **2009**, *5*, 126–134.
- (37) Yu, M.; Zheng, J. Clearance Pathways and Tumor Targeting of Imaging Nanoparticles. *ACS Nano* **2015**, *9*, 6655–6674.
- (38) Lee, T. Y.; Liu, M. S.; Huang, L. J.; Lue, S. I.; Lin, L. C.; Kwan, A. L.; Yang, R. C. Bioenergetic Failure Correlates with Autophagy and Apoptosis in Rat Liver Following Silver Nanoparticle Intraperitoneal Administration. *Part. Fibre Toxicol.* **2013**, *10*, 40.
- (39) Patlolla, A. K.; Hackett, D.; Tchounwou, P. B. Silver Nanoparticle-Induced Oxidative Stress-Dependent Toxicity in Sprague-Dawley Rats. *Mol. Cell. Biochem.* **2015**, *399*, 257–268.
- (40) Sahu, S. C.; Njoroge, J.; Bryce, S. M.; Zheng, J.; Ihrie, J. Flow Cytometric Evaluation of the Contribution of Ionic Silver to Genotoxic Potential of Nanosilver in Human Liver HepG2 and Colon Caco-2 Cells. *J. Appl. Toxicol.* **2016**, *36*, 521–531.
- (41) Pelley, J. L.; Daar, A. S.; Saner, M. A. State of Academic Knowledge on Toxicity and Biological Fate of Quantum Dots. *Toxicol. Sci.* **2009**, *112*, 276–296.
- (42) Loginova, Y. F.; Dezhurov, S. V.; Zherdeva, V. V.; Kazachkina, N. I.; Wakstein, M. S.; Savitsky, A. P. Biodistribution and Stability of CdSe Core Quantum Dots in Mouse Digestive Tract Following *per os* Administration: Advantages of Double Polymer/Silica Coated Nanocrystals. *Biochem. Biophys. Res. Commun.* **2012**, *419*, 54–59.
- (43) Vasudevan, D.; Gaddam, R. R.; Trinchia, A.; Cole, I. Core–Shell Quantum Dots: Properties and Applications. *J. Alloys Compd.* **2015**, *636*, 395–404.
- (44) Feliu, N.; Docter, D.; Heine, M.; Pino, P. D.; Ashraf, S.; Kolosnjaj-Tabi, J.; Macchiarini, P.; Nielsen, P.; Alloyeau, D.; Gazeau, F.; Stauber, R. H.; Stauber, R. H.; Parak, W. J. *In vivo* Degeneration and the Fate of Inorganic Nanoparticles. *Chem. Soc. Rev.* **2016**, *45*, 2440–2457.